Available online at www.sciencedirect.com
SCIENCE DIRECT®
Sensors and Actuators A 104 (2003) 151–161
SENSORS AND ACTUATORS A PHYSICAL
www.elsevier.com/locate/sna

Analytical analysis of a circular PZT actuator for valveless micropumps

Shifeng Li, Shaochen Chen*

Mechanical Engineering Department, The University of Texas at Austin, 1 University Station, ETC 5.160, Austin, TX 78712, USA

Received 29 May 2002; received in revised form 13 January 2003; accepted 19 January 2003

Abstract

Closed form analytical equations are important tools for predicting and optimizing the behavior of a piezoelectric microactuator for micropump applications. However, there is no reliable analytical solution to date to analyze the behavior of a circular piezoelectric microactuator for a valveless micropump. In this paper, a linear strain distribution is assumed across the thickness of the passive plate of the lead zirconate titanate (PZT) actuator given that the mechanical properties such as Young's modulus and Poisson ratio of the actuator and the passive plate are close. An analytical equation for the passive plate deflection is derived upon this assumption. The analytical result shows excellent agreement with experimental data as well as the results from finite element simulation. Based on this analytical model, the effects of several important parameters and nondimensional variable groups on the actuator performance have been investigated. These parameters and variables include the dimensions and mechanical properties of the PZT disk, the passive plate, and the bonding layer material.

Keywords: Analytical analysis; PZT actuator; Valveless micropump; MEMS

1. Introduction

Piezoelectric actuators have been widely used in mechanical actuation and sound generating or receiving devices [1]. To predict and optimize the behavior of the piezoelectric actuator, Crawley and Anderson developed an analytical model for a PZT actuator based on a uniform strain assumption [2]. This model is valid for a thin piezo-disk, where the disk thickness is less than half of the passive plate thickness. Kim and Jones used a linear strain assumption to predict an optimal rectangular actuator-to-plate thickness ratio at different Young's modulus ratios by optimizing the moment applied by a dual layer piezoelectric actuator [3]. The linear strain assumption provided a good approximation for the rectangular shape actuator when the bonding layer is thin. Ray et al. conducted three-dimensional analytical analysis for a rectangular, simply supported, multiple-layer piezoelectric passive plate [4]. Chaudhry and Rogers presented a mathematical model for determining the optimum thickness ratio. They also predicted optimal length ratios for a rectangular actuator patch on a rectangular plate with fixed boundary [5]. For a circular bimorph, Yanagisawa and Nakagawa presented an analytical equation to optimize the radius of a resonant piezoelectric actuator with a limited number of thickness ratios [6]. Dobrucki and Pruchnicki studied an axisymmetric bimorph using a finite element method. An analytical model was also presented for the deflection of the bimorph with the piezoelectric element covering the entire plate. A free boundary was assumed in their work [7]. Tzou [8] and Larson [9] conducted comprehensive investigation on composite piezoelectric shell models with various shapes and applications. A comprehensive review of analytical and numerical approaches to model and optimize PZT actuator behavior was recently given by Chee et al. [1].

In the micro-electro-mechanical systems (MEMS) area, a piezoelectric actuator has also been widely used in micropumps and other actuation devices [10,11,14]. Yoon and Washington proposed moment balance method to analyze beam type piezoelectric actuator [13]. DeVoe et al. derived an analytical model for a beam type of piezoelectric microactuators that included the bonding layer effects [11,12]. Cao et al. presented a simplified analytical model for a thin passive plate type of piezoelectric microactuators in valveless micropump applications. In order to obtain a closed form analytical solution, major assumptions such as the entire passive plate to be covered by a PZT layer and no transverse shear have to be made [15]. Such assumptions may result in a significant discrepancy between the analytical results and experimental results [15,16]. For this reason, a finite element method has been the main approach to

* Corresponding author. Tel.: +1-512-232-6094; fax: +1-512-471-1045.
E-mail address: scchen@mail.utexas.edu (S. Chen).

0924-4247/03/$ – see front matter © 2003 Elsevier Science B.V. All rights reserved.
doi:10.1016/S0924-4247(03)00006-2

analyze and optimize the piezoelectric microactuator consisting of a PZT disk, bonding material, and a passive plate [7,14].

In this paper, a new analytical equation is derived based on linear strain assumptions to analyze the passive plate deflection in a piezoelectric microactuator. Results from this equation are compared with previously published experimental data and finite element simulation. Furthermore, the analytical model is used to investigate the effects of several critical design parameters and nondimensional variable groups on the performance of the actuator.

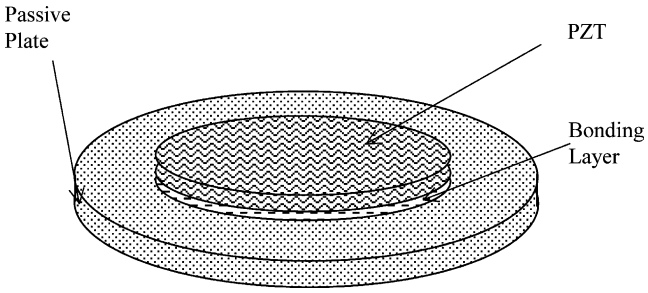

Fig. 1. Schematic of a single piezoelectric layer micropump actuator.

2. Analytical analysis of the single piezoelectric actuator

A typical PZT-actuated valveless micropump is shown in Figs. 1 and 2 [10,17–19]. The PZT disk is bonded to the passive plate using a thin layer of conducting epoxy. When an electric filed is applied to the PZT disk, the strain produced in the PZT disk causes the passive plate to expand or contract, resulting in actuation for the micropump. Therefore, the liquid can be pumped in or out of the chamber. A net flow is formed from the inlet to the outlet due to the function of the diffuser or nozzle depending on the flow direction. For convenience of analysis, we divided this structure into two parts: one is the three-layer structure including the PZT disk, the bonding material, and the passive plate beneath the bonding layer, the other is the rest of the passive plate part. The moment balance for each part is shown in Fig. 3.

As shown in Fig. 4, there exists a neutral surface that does not have transverse strain or radial strain. The potential energy in the neutral surface reaches a minimum value [7]. The location of this neutral surface is found to be

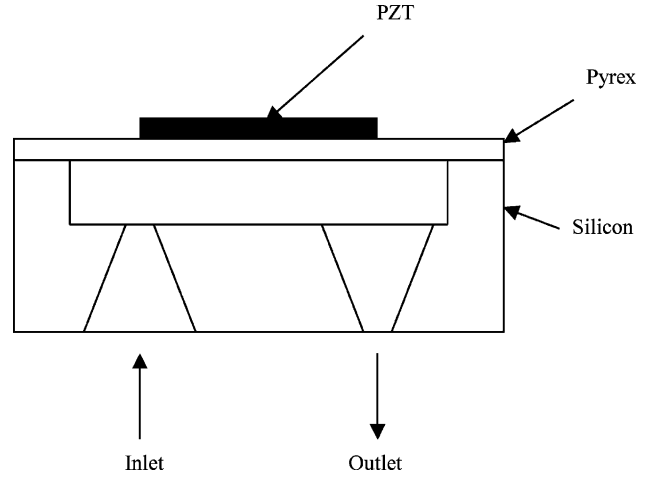

Fig. 2. The PZT actuation valveless micropump schematics.

where E represents the Young' modulus, γ is the Poisson ratio, and h is the thickness. The subscript p, b, and pzt represent the passive plate, the bonding layer, and the PZT disk, respectively.

$$h = \frac{1}{2}\frac{(E_p h_p^2/(1-\gamma_p^2)) + (E_b[(h_b+h_p)^2 - h_p^2]/(1-\gamma_b^2)) + (E_{pzt}[(h_b+h_p+h_{pzt})^2 - (h_p+h_b)^2]/(1-\gamma_{pzt}^2))}{(E_p h_p/(1-\gamma_p^2)) + (E_b h_b/(1-\gamma_b^2)) + (E_{pzt} h_{pzt}/(1-\gamma_{pzt}^2))} \quad (1)$$

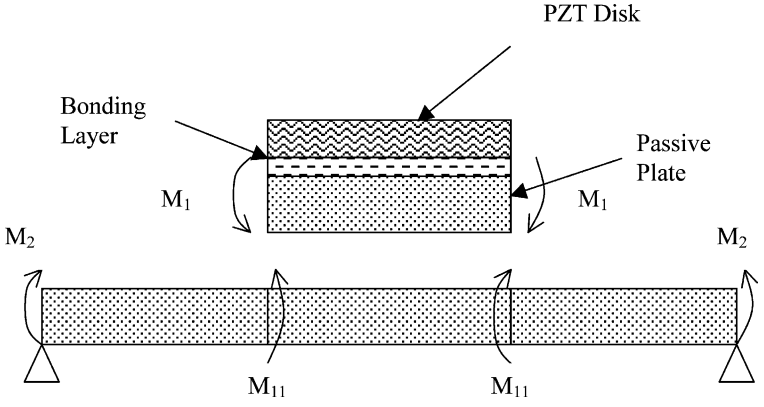

Fig. 3. Moment balance of the piezoelectric microactuator.

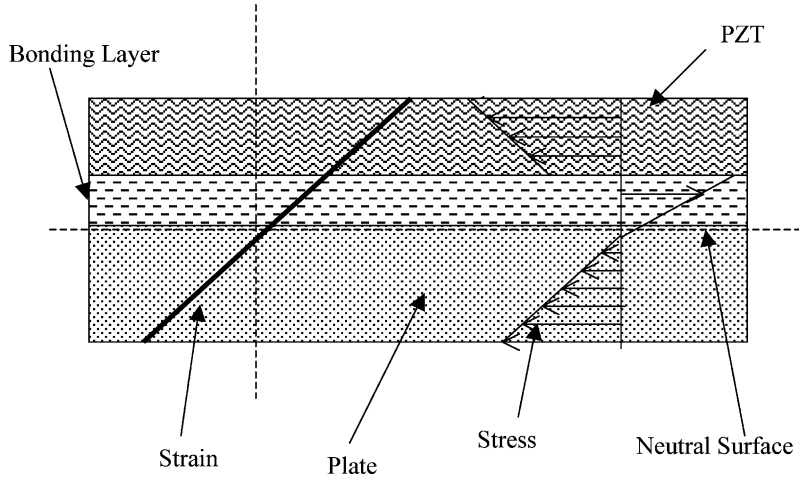

Fig. 4. Linear strain distribution and nonlinear stress distribution in the passive plate, the bonding layer, and the PZT disk.

For most valveless micropumps developed, a Pyrex 7740 glass wafer is used to bond with the silicon substrate to seal the pumping chamber [10,17–19]. The Young's modulus and Poisson ratio of the Pyrex 7740 glass material are close to those of the PZT material. Given that the three-layer structure is thin compared to its radius of curvature, a linear strain distribution across the thickness direction can be assumed in this structure. Therefore, the strain at the interface will be continuous and the radius of curvature for each layer shares the same center.

For the bonding material, the stress follows

$$\sigma_b = \frac{E_b}{1-\gamma_b}\varepsilon_b \tag{2}$$

where ε_b is the strain of the bonding material. Since the strain distribution is assumed to be linear, we have

$$\varepsilon(z) = \varepsilon_p = \varepsilon_b = \varepsilon_{pzt} = z\kappa \tag{3}$$

$$\sigma_p = \frac{\sigma_i}{h_p - h} z \tag{4}$$

where z is the deflection from the neutral surface, σ_i the stress at the interface between the bonding layer and the passive plate, and h is the distance between the neutral surface and the bottom surface of the passive plate. The passive plate, the bonding layer, and the PZT disk have different deflection from the neutral surface. The strain slope is given by

$$\kappa = \frac{1-\gamma_p}{E_p}\frac{\sigma_i}{h_p - h} \tag{5}$$

The stress distribution in the bonding layer follows

$$\sigma_b = \frac{E_b}{1-\gamma_b}\kappa z = \frac{1-\gamma_p}{1-\gamma_b}\frac{E_b}{E_p}\frac{\sigma_i}{h_p - h} z \tag{6}$$

For an actuator with a single piezoelectric layer, the PZT disk has five independent elastic material constants and three independent piezoelectric constants. However, because the strains in the z-direction cannot generate traction forces at the interface surfaces and the micropump working frequency is much lower than the resonant frequency of the PZT actuator that is typically over 1 MHz, the PZT material is assumed to be elastically isotropic. From the linear piezoelectric constitutive equations, the stress and strain relationship for the PZT-actuator can be expressed as

$$\begin{aligned}\sigma_{pzt} &= \frac{E_{pzt}}{1-\gamma_{pzt}}\left(\kappa z - \frac{V}{h_{pzt}} d_{31}\right) \\ &= \frac{\sigma_i(1-\gamma_p)E_{pzt_i}}{(1-\gamma_{pzt})E_p(h_p - h)} z - \frac{E_{pzt}}{1-\gamma_{pzt}}\frac{V}{h_{pzt}} d_{31}\end{aligned} \tag{7}$$

where d_{31} is the electrical–mechanical coupling coefficient in the z-direction and V is the working voltage.

Balancing the moment in the three-layer structure gives

$$\int_{-h}^{h_p-h} \sigma_p z\,dz + \int_{h_p-h}^{h_p-h+h_b} \sigma_b z\,dz + \int_{h_p-h+h_b}^{h_p-h+h_b+h_{pzt}} \sigma_{pzt} z\,dz = 0 \tag{8}$$

Let $h' = h_p - h$, we have

$$\begin{aligned}\sigma_i = \frac{3\eta V d_{31}(2h' + 2h_b + h_{pzt})h'}{2(h'^3 + h^3 + \alpha((h' + h_b)^3 - h'^3) \\ + \beta((h' + h_b + h_{pzt})^3 - (h' + h_b)^3))}\end{aligned} \tag{9}$$

where $\alpha = ((1-\gamma_p)/(1-\gamma_b))(E_b/E_p)$, $\beta = ((1-\gamma_p)/(1-\gamma_{pzt}))(E_{pzt}/E_p)$ and $\eta = E_{pzt}/(1-\gamma_{pzt})$.

The moment M_1 is given by

$$\begin{aligned}M_1 &= \int_{-h}^{h'} \sigma_p z\,dz \\ &= \frac{\eta V d_{31}(2h' + 2h_b + h_{pzt})(h'^3 + h^3)}{2(h'^3(1-\alpha) + h^3 + (\alpha - \beta)(h' + h_b)^3 \\ &\quad + \beta(h' + h_b + h_{pzt})^3)}\end{aligned} \tag{10}$$

Following Christensen's work [20], we derived the Young's modulus and the Poisson ratio for the three-layer structure. For the PZT and the bonding layer

$$E' = C_1 E_{pzt} + C_2 E_b + \frac{C_1 C_2 E_{pzt} E_b (\gamma_{pzt} - \gamma_b)^2}{C_1 E_{pzt}(1-\gamma_b{}^2) + C_2 E_b (1-\gamma_{pzt}{}^2)} \tag{11}$$

$$\gamma' = \frac{C_1 \gamma_{pzt} E_{pzt}(1-\gamma_b{}^2) + C_2 \gamma_b E_b (1-\gamma_{pzt}{}^2)}{C_1 E_{pzt}(1-\gamma_b{}^2) + C_2 E_b (1-\gamma_{pzt}{}^2)} \tag{12}$$

where $C_1 = h_{pzt}/h''$ and $C_2 = h_b/h''$, $h'' = h_{pzt} + h_b$.

Now let $h_{all} = h_{pzt} + h_b + h_p$, the Young's modulus E_c and Poisson ratio γ_c for this three-layer structure are

$$E_c = C_1{}'E' + C_2{}'E_p + \frac{C_1{}'C_2{}'E'E_p(\gamma_p - \gamma')^2}{C_1{}'E_p(1-\gamma'^2) + C_2{}'E'(1-\gamma_p^2)} \tag{13}$$

$$\gamma_c = \frac{C_1{}'\gamma_p E_p(1-\gamma'^2) + C_2{}'\gamma' E'(1-\gamma_p^2)}{C_1{}'E_p(1-\gamma'^2) + C_2{}'E'(1-\gamma_p^2)} \tag{14}$$

where $C_1{}' = h_p/h_{all}$ and $C_2{}' = h''/h_{all}$.

For the passive plate, a general solution for its deflection W_1 is given by [21]

$$W_1(r) = \frac{M_{11} b^2}{2D_p((1-\gamma_p)a^2 + (1+\gamma_p)b^2)} \times \left[-r^2 + 2a^2 \log\frac{r}{a} + a_2\right] \tag{15}$$

where a is the diameter of the passive plate and b is the diameter of the PZT and the flexural modulus for the passive plate D_p is given by

$$D_p = \frac{E_p h^3}{12(1-\gamma_p^2)} \tag{16}$$

The deflection W_2 for the multiple-layer follows [21]

$$W_2(r) = \frac{M_{11} b^2}{2D_p((1-\gamma_p)a^2 + (1+\gamma_p)b^2)} \times \left[-b^2 + 2a^2 \log\frac{b}{a} + a^2\right] + \frac{M_1}{2D_c(1+\gamma_c)}(b^2 - r^2) \tag{17}$$

where the flexural modulus for the multi-layer structure D_c is given by

$$D_c = \frac{E_c h^3}{12(1-\gamma_c^2)} \tag{18}$$

From the continuity condition

$$\left.\frac{dw_1}{dr}\right|_{r=b} = \left.\frac{dw_2}{dr}\right|_{r=b} \tag{19}$$

The moment M_{11} is found to be

$$M_{11} = -\frac{M_1 D_p((1-\gamma_p)a^2 + (1+\gamma_p)b^2)}{D_c(1+\gamma_c)(a^2 - b^2)} \tag{20}$$

From Eqs. (15) and (17), it is easy to see that the dimensions of the PZT, the passive plate and the bonding

Table 1
Properties of the PZT, conductive epoxy and passive plate

	Property	Tensor (in order of x, y, z, xy, yz and xz)
PZT	Piezoelectricity $\boldsymbol{e}$ (C m^{-2})	$\begin{bmatrix} 0 & 0 & -5.4 \\ 0 & 0 & -5.4 \\ 0 & 0 & 15.8 \\ 0 & 0 & 0 \\ 0 & 12.3 & 0 \\ 12.3 & 0 & 0 \end{bmatrix}$
	Permittivity $\boldsymbol{\varepsilon}$ (F m^{-1})	$\begin{bmatrix} 8.107 & 0 & 0 \\ 0 & 8.107 & 0 \\ 0 & 0 & 7.346 \end{bmatrix} \times 10^{-9}$
	Compliance $\boldsymbol{S}$ (m^2 N^{-1})	$\begin{bmatrix} 16.4 & -5.75 & -8.45 & 0 & 0 & 0 \\ 0 & 16.4 & -8.45 & 0 & 0 & 0 \\ & & 18.8 & 0 & 0 & 0 \\ & & & 44.3 & 0 & 0 \\ & \text{symmetric} & & & 47.5 & 0 \\ & & & & & 47.5 \end{bmatrix} \times 10^{-12}$
Epoxy	Young's modulus $\boldsymbol{E}$ (GPa)	5.17
	Poisson ratio $\boldsymbol{\gamma}$	0.3
Glass	Young's modulus $\boldsymbol{E}$ (GPa)	62.75
	Poisson ratio $\boldsymbol{\gamma}$	0.2

layer and their Young's modulus have a significant influence on the magnitude of the microactuator deflection. Meanwhile, some nondimensional variables such as $(b/a)^2$, $E_b h_b^3/E_p h_b^3$, and $E_{pzt} h_{pzt}^3/E_p h_p^3$ are expected to have effects on the performance of the piezoelectric microactuator. Details will be discussed in the following section.

Table 2
Dimensions for the piezoelectric actuator simulation

The passive plate diameter a (mm)	6.0
The passive plate thickness h_p (μm)	500
Piezoelectric disk diameter b (mm)	4.0–5.0
Piezoelectric disk thickness h_{pzt} (μm)	200
Bonding layer thickness h_b (μm)	20

3. Results and discussion

3.1. Comparison with data from experiments and finite element simulation

The analytical equation derived in the previous section allows one to directly predict the performance of the piezoelectric actuator. However, such analytical solution needs to be verified first since the derivation process involves a major assumption of linear strain distribution between the PZT disk, the bonding material, and the passive plate. One effective way to verify this analytical solution is to compare it with the results from FEM. Due to dimensional symmetry, only a quarter of the piezoelectric actuator is considered in this paper using a commercial FEM package, Ansys 5.7 with fixing and symmetrical boundaries. The 10-node Solid-92 is chosen to model the passive plate and the bonding layer. The coupled field scalar Solid-98 is used to model the PZT layer. There are approximately 4000 elements in this model. Another way to verify this analytical equation is to compare its results with available experimental data using the same dimensions and materials for the PZT disk, the bonding material, and the passive plate [14]. The properties for the PZT (PZT-5A), the conductive epoxy (EPO-TEK H31), and the passive plate are summarized in Table 1. The piezoelectric microactuator dimensions are listed in Table 2. The working voltage is 50 V (zero-to-peak).

The passive plate deflection from the analytical solution, the FEM simulation, and experimental results is shown in Fig. 5. The maximum deflection at the center of the passive plate from the analytical equation is 0.1788 μm and the deflection from the FEM simulation is 0.1829 μm, resulting in a discrepancy less than 3%. The bonding process during the micropump fabrication often introduces some residual thermal stress. From simulation, a tensile residual stress of 1 MPa is found inside the passive plate. After including this stress, we found that the passive plate deflection from our analytical prediction agrees well with experiment study. This suggests that the analytical equation derived in this work is valid.

We also extended the investigation to other bonding materials and passive plates by comparing the analytical results with those from the FEM simulation. Because typical

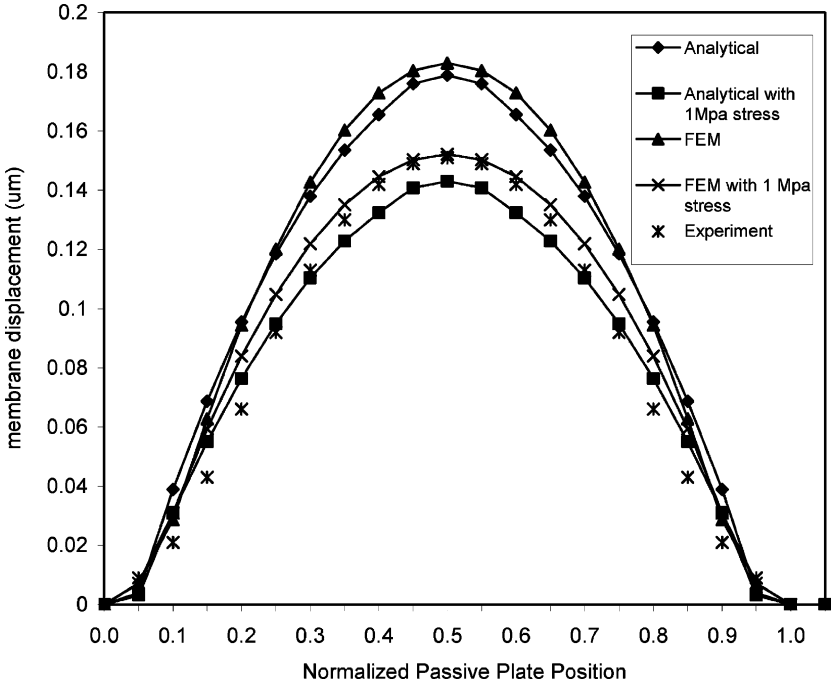

Fig. 5. The passive plate profile from analytical calculation, experimental data, and FEM simulation. The working voltage $V_{0\text{-}p} = 50$ V, the bonding layer thickness ratio $h_{b\text{-}p} = 0.04$, and the passive plate thickness $h_p = 500$ mm.

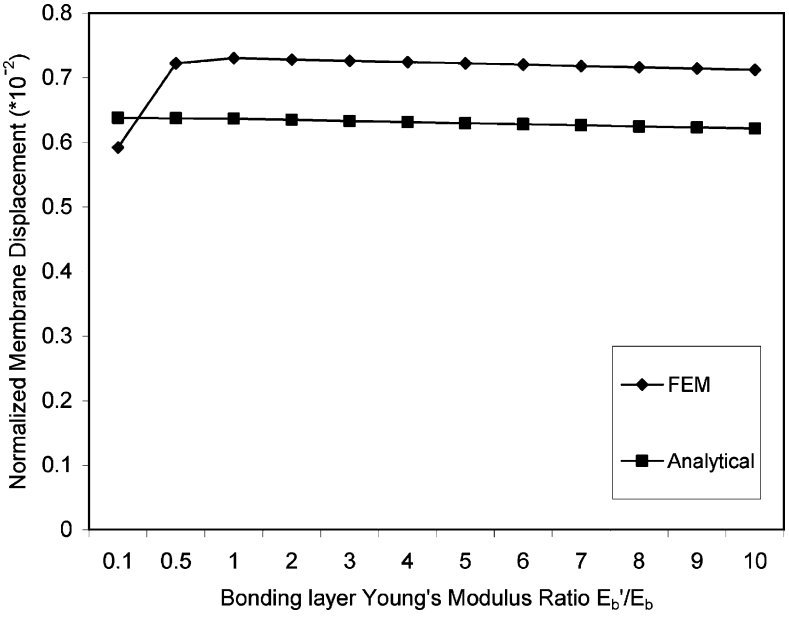

Fig. 6. Results from FEM and analytical calculation with different Young's modulus, normalized with the passive plate thickness $h_p = 500$ mm.

Poisson ratio of materials is from 0.2 to 0.3, the passive plate deflection change due to Poisson ratio variation is less than 3%. Therefore, only the Young's modulus effect is investigated. We found that there is no significant error from this analytical solution if we change the Young's modulus of the bonding layer from 0.5 to 10 times that of the current one (Fig. 6). However, when this Young's modulus ratio is below 0.2, the linear strain assumption in deriving the analytical solution is not valid any more. For the passive plate plates of various Young's modulus from 30 to 600 GPa, Fig. 7 suggests this analytical equation is able to predict reasonable passive plate deflections. But if this ratio is below 0.5, this analytical equation fails to predict accurate passive plate deflection since the linear strain assumption is not valid. From a practical point of view, this range of Young's modulus (from 30 to 600 GPa) covers almost all possible MEMS plate materials such as glass, silicon, silicon nitride, and most metals.

3.2. PZT disk effects

The PZT disk is an important element in a piezoelectric actuator. The dimensions of the PZT disk play a significant

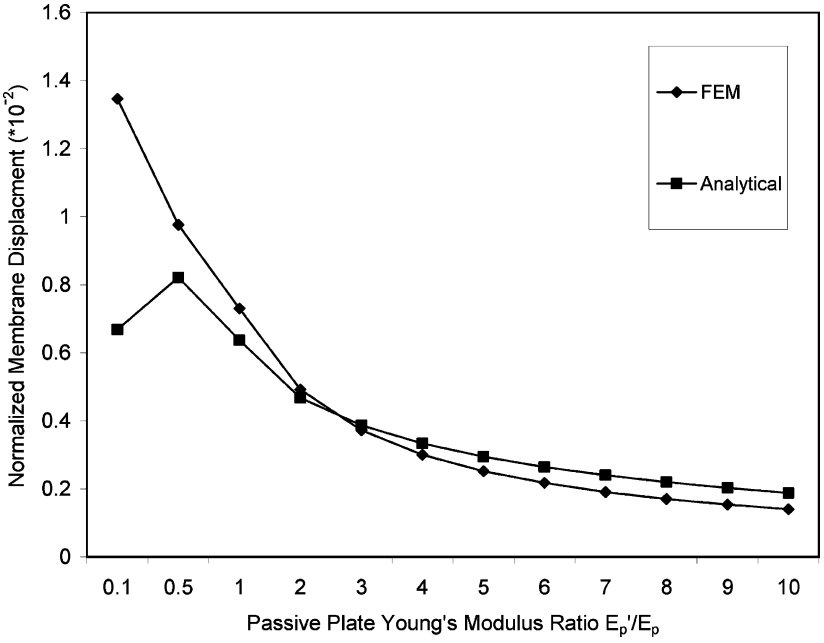

Fig. 7. Results from FEM and analytical equation with different passive plate Young's modulus E_p.

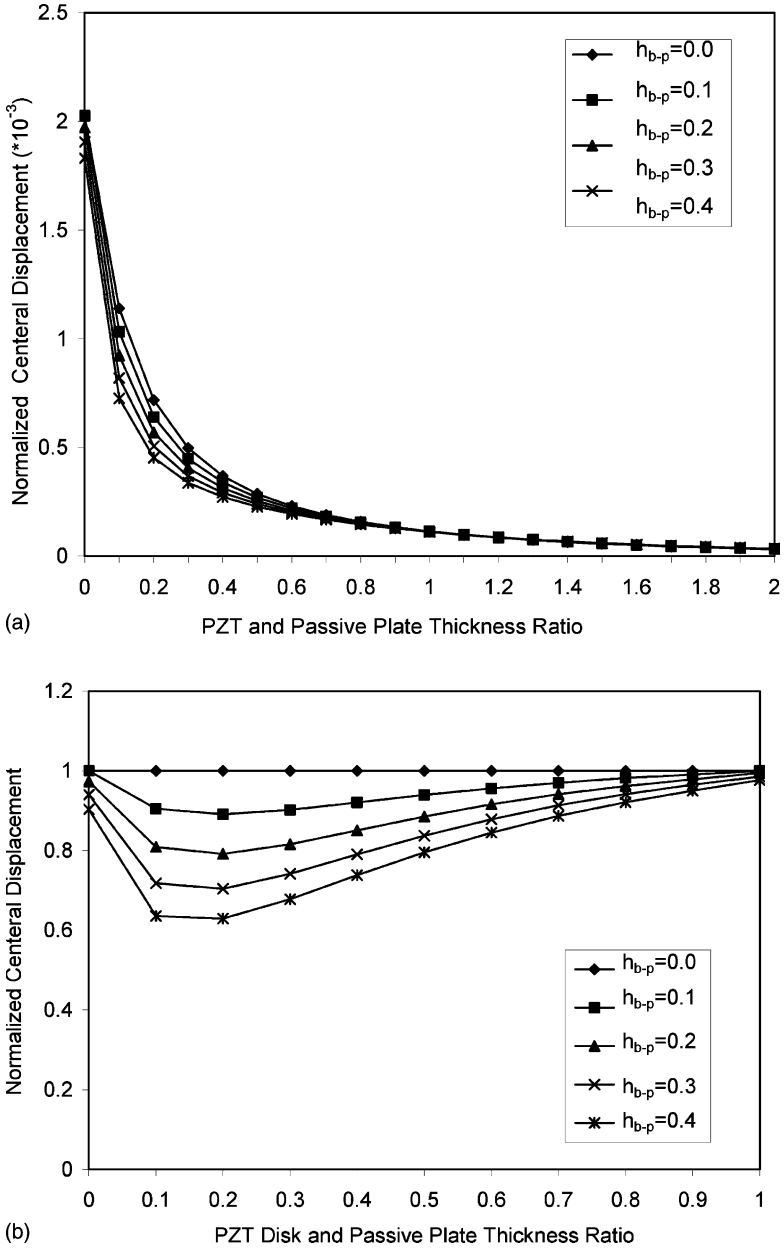

Fig. 8. The center passive plate deflections at different PZT disk thickness, (a) normalized with the passive plate thickness $h_p = 500$ μm, (b) normalized with the case that the bonding layer thickness ratio $h_{b\text{-}p} = 0$.

role in the actuator design. Practically, the bonding layer is less than 100 mm (typically around 20 mm), and rather thin compared to the passive plate. Therefore, we investigated the PZT/passive plate thickness ratio effect on the passive plate deflection for bonding layer/plate thickness ratio $h_{b\text{-}p}$ ranging from 0 to 0.4 as shown in Fig. 8a. We found that the passive plate deflection decreases when increasing the bonding layer/passive plate thickness ratio $h_{b\text{-}p}$ and increasing the PZT/passive plate thickness ratio. For the PZT/passive plate thickness ratio less than 0.5, the bonding material thickness effect becomes important. In order to find the bonding layer effect in detail, the data is normalized with the passive plate deflection with no bonding layer. Fig. 8b shows the bonding layer effect is the strongest when the PZT thickness ratio is around 0.15. However, when this thickness ratio is beyond 0.8, the bonding layer effect is limited. In Fig. 9a, the passive plate deflection increases when the square of the PZT/passive plate radius ratio increases, but decreases with the bonding material thickness ratio $h_{b\text{-}p}$. In Fig. 9b, when the bonding layer thickness ratio is larger than 0.3, the passive plate deflection drops down to a value of 80% of the passive plate deflection without the bonding layer. This result implies the bonding layer reduces the passive plate

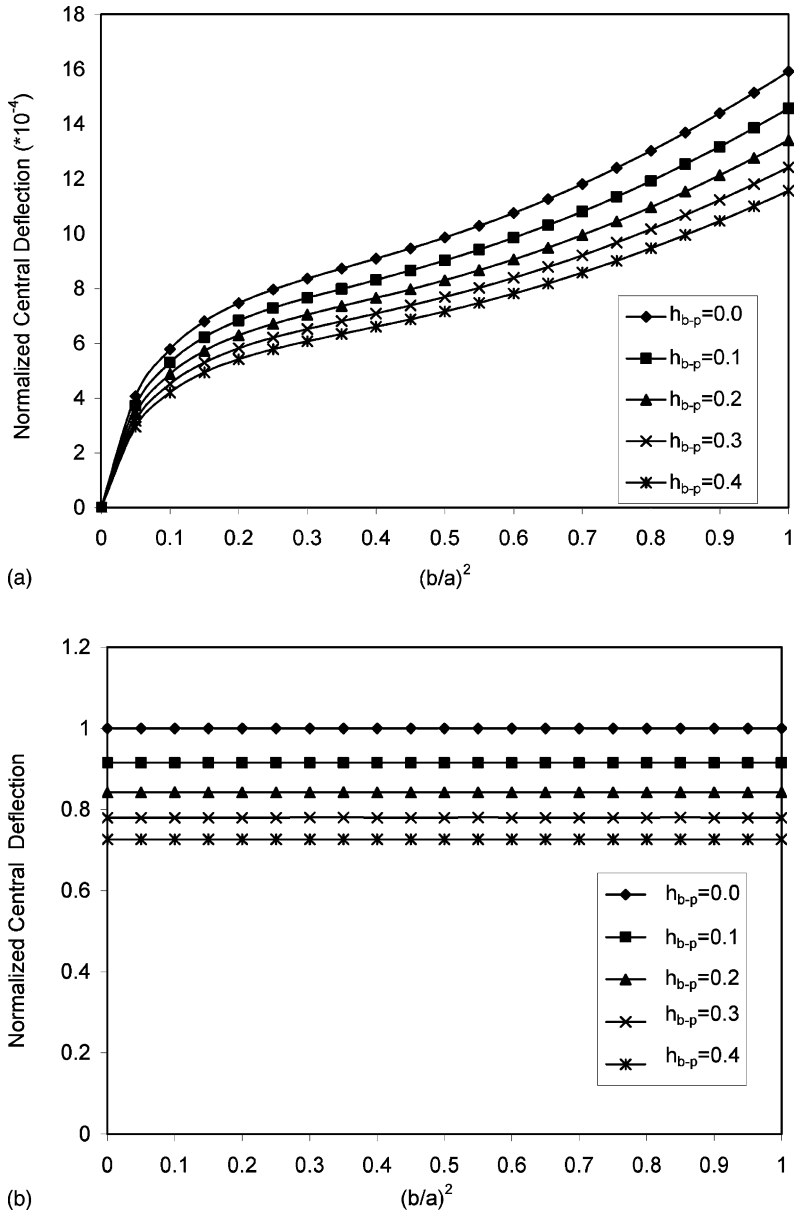

Fig. 9. The passive plate center deflection at different radius ratio of PZT disk and the passive plate, (a) normalized with the passive plate thickness $h_p = 500$ mm, (b) normalized with the case that the bonding layer thickness ratio $h_{b\text{-}p} = 0$.

deflection significantly when the bonding layer thickness ratio is above 0.3.

3.3. Bonding material effects

In previous studies of developing analytical solutions for circular piezoelectric microactuators, the bonding layer effects on the actuator performance were usually neglected in order to simplify the model [15,16]. The analytical solution derived in this work allows one to investigate the bonding layer material effect including its dimensions and Young's modulus as shown in Fig. 10. Increasing the bonding material thickness will reduce the passive plate deflection, but when the PZT/passive plate thickness ratio $h_{pzt\text{-}p}$ is above 0.4, the maximum passive plate deflection does not show a significant change. This implies the bonding material effect is limited and negligible for a thick PZT actuator. However, for a thin PZT disk (e.g. less than 200 mm thick), we found that the bonding material effect cannot be neglected. But this does not mean the thinner PZT gives a larger deflection. We performed this analysis under a constant voltage. In practice, a piezoelectric material has maximum allowable field strength. If this maximum allowable field strength is exceeded, the material will degrade and eventually lose its piezoelectric properties. If the electric filed remains constant, there exists an optimal PZT thickness for the specific bonding

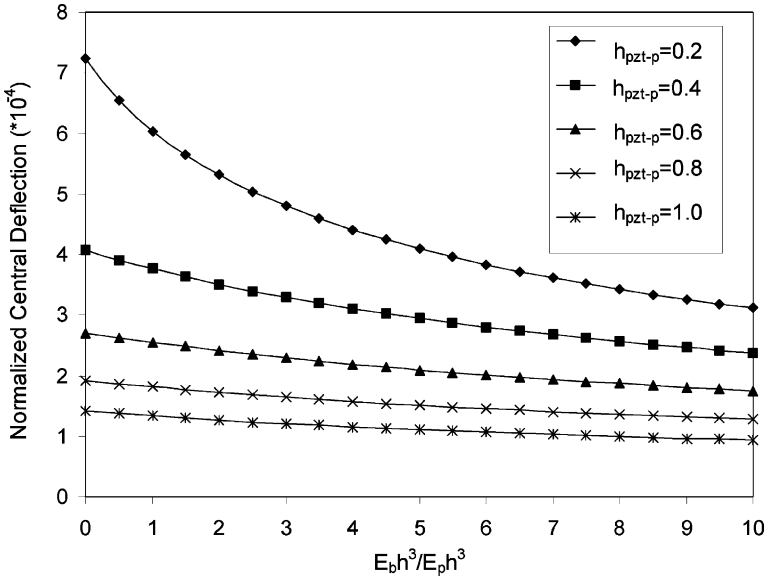

Fig. 10. The passive plate center deflections at different $E_b h^3/E_p h^3$ ratio, normalized with the passive plate thickness $h_p = 500$ μm.

layer thickness ratio as depicted in Fig. 11. Moreover, there is a slight increase of this optimal PZT disk thickness when the bonding layer thickness increases.

3.4. Passive plate effects

The passive plate dimensions also have an important role on the actuator performance. Considering practical applications, we focus the study on passive plate thickness and diameter ratio from 0 to 0.5. Meanwhile, the PZT diameter effect is coupled in this investigation with the PZT and the passive plate diameter ratio $R_{pzt\text{-}p}$ ranging from 0.2 to 1.0. In Fig. 12, the maximum achievable passive plate deflection reaches a peak when the passive plate thickness/diameter ratio is around 0.01–0.02. Although this ratio is not practically useful for actuator design, this analytical solution does suggest that in order to enhance the performance of the single layer piezoelectric actuator, the passive plate thickness/diameter ratio needs to be as close to 0.02 as possible. Also, a larger diameter PZT disk will yield bigger deflection.

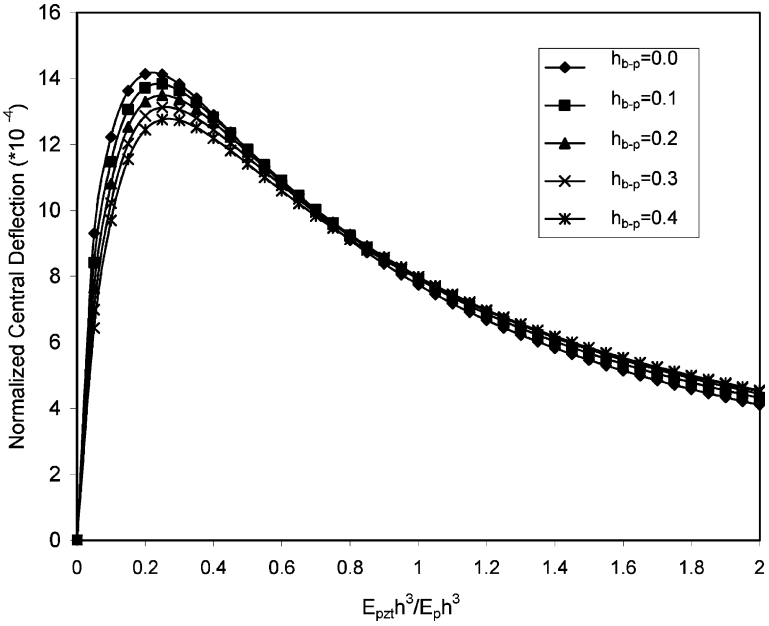

Fig. 11. The passive plate center deflections at different $E_{pzt} h^3/E_p h^3$ ratio under a constant electrical field, normalized with the passive plate thickness $h_p = 500$ μm.

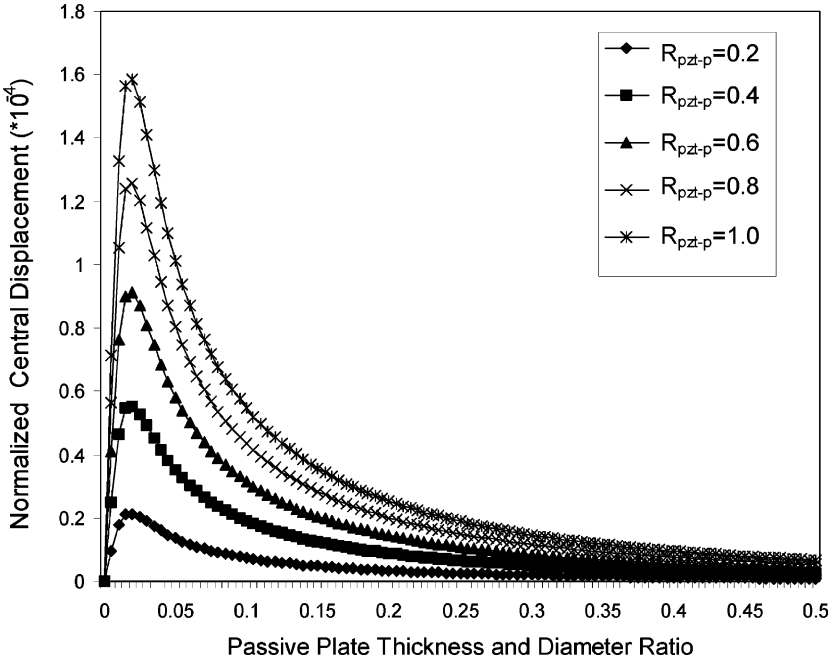

Fig. 12. The passive plate central deflection at different passive plate dimensions, normalized with the plate diameter $a = 6$ mm.

4. Conclusions

An analytical equation for the analysis of a PZT actuator was derived based on an assumption of linear strain distribution along the PZT disk, the bonding layer, and the passive plate. Results from both FEM simulation and experiment data verified that this analytical equation is valid. One important aspect of this analytical solution is that it can predict the performance of the PZT actuator system with different design parameters and operation conditions, and therefore allow one to optimize the design. The dimensions and properties of the PZT disk play a significant role in the actuator performance. The passive plate deflection decreases as the PZT thickness and bonding material thickness increase and increases as the PZT radius increases. The bonding layer effects become important for a thin PZT disk. The mechanical properties such as the Young's modulus also have certain effects on the passive plate deflection. When the electric field is kept constant, there exists an optimal PZT thickness. When the bonding layer thickness increases, this optimal PZT thickness also increases. Moreover, this analytical solution suggests that an optimal value for the passive plate thickness/diameter ratio is about 0.02 in order to get high performance actuator design.

References

[1] C.Y.K. Chee, L. Tong, G.P. Steven, A review on the modeling of piezoelectric sensors and actuators incorporated in intelligent structures, J. Intell. Mater. Syst. Struct. 9 (1998) 3–19.

[2] E.F. Crawley, E.H. Anderson, Detailed models of piezoceramic actuation of beam, J. Intell. Mater. Syst. Struct. 1 (1990) 4–25.

[3] S.J. Kim, J.D. Jones, Optimal design of piezoactuators for active noise and vibration control, AIAA J. 29 (1991) 2047–2053.

[4] M.C. Ray, R. Bhattacharya, B. Samanta, Exact solutions for static analysis of intelligent structures, AIAA J. 31 (1993) 1684–1691.

[5] Z. Chaudhry, C.A. Rogers, Performance and optimization of induced strain actuated structures under external loading, AIAA J. 32 (1994) 1289–1294.

[6] T. Yanagisawa, Y. Nakagawa, Determination of optimum dimension for unimorph type piezoelectric loudspeaker, Trans. Inst. Electron. Informat. Commun. Eng. A J. 76 (1993) 1261–1269.

[7] A.B. Dobrucki, P. Pruchnicki, Theory of piezoelectric axisymmetric bimorph, Sens. Actuators A 58 (1997) 203–212.

[8] H.S. Tzou, Piezoelectric Shells: Distributed Sensing and Control of Continua, Kluwer Academic Publishers, Dordrecht, 1994.

[9] P.H. Larson, The Use of Piezoelectric Materials in Creating Adaptive Shell Structures, Ph.D. Thesis, University of Delaware, 1994.

[10] E. Stemme, G. Stemme, A valve-less diffuser/nozzle based fluid pump, Sens. Actuators A 39 (1993) 159–167.

[11] D.L. DeVoe, A.P. Pisano, Modeling and optimal design of piezoelectric cantilever microactuators, J. Microelectromech. Syst. 6 (1997) 266–270.

[12] D.L. DeVoe, A.P. Pisano, Surface micromachined piezoelectric accelerometers, J. Microelectromech. Syst. 10 (2001) 180–186.

[13] H.S. Yoon, G. Washington, Piezoceramic actuated aperture antennae, Smart Mater. Struct. 7 (1998) 537–542.

[14] C.J. Morris, F.K. Forster, Optimization of a circular piezoelectric bimorph for a micropump driver, J. Micromech. Microeng. 10 (2000) 459–465.

[15] L. Cao, S. Mantell, D. Polla, Design and simulation of an implantable medical drug delivery system using microelectromechanical systems technology, Sens. Actuators A 94 (2001) 1–9.

[16] S.F. Li, Y. Liu, S.C. Chen, Dynamic modeling and optimization of a valveless PZT actuated micropump, Proc. SPIE 4560 (2001) 67–74.

[17] T. Gerlach, H. Wurmus, Working principle and performance of the dynamic micropump, Sens. Actuators A 50 (1995) 135–140.

[18] A. Olsson, G. Stemme, E. Stemme, A valve-less planar fluid with two pump chambers, Sens. Actuators A 46/47 (1995) 549–556.
[19] E.K. Forster, R.L Bardell, M.A. Abramowitz, N.R. Sharma, A. Blanchard, in: Proceedings of IMECE, ASME on Design, Fabrication and Testing of Fixed Valve Micropumps, 1995.
[20] R.M. Christensen, Mechanics of Composite Materials, Wiley, New York, 1979.
[21] S. Timoshenko, S. Woinowsky-Krieger, Theory of Plates and Shells, second ed., McGraw-Hill, New York, 1995.

Biographies

Shifeng Li received his BS and MS in mechanical engineering from Shanghai Jiaotong University, PR China in 1994 and 1999, respectively. Currently, he is graduate student in the Mechanical Engineering Department at the University of Texas at Austin, working on design, fabrication and simulation of microfluidic devices and other MEMS devices.

Shaochen Chen received his PhD in mechanical engineering from the University of California at Berkeley in 1999. Currently, He is an assistant professor of the Mechanical Engineering Department at the University of Texas at Austin. His research interest lies in MEMS, laser materials processing, and thermal/fluid transport in micro- and nano-systems. His research applications include microelectronics, biomedical engineering, and life science. He received a CAREER award from the US National Science Foundation in 2001 and an Outstanding Young Manufacturing Engineer award from the Society of Manufacturing Engineers in 2002.